Electron-impact rotational excitation of water

Alexandre Faure,[1] Jimena D. Gorfinkiel[2] and Jonathan Tennyson[2]⋆

[1]*Laboratoire d'Astrophysique, Observatoire de Grenoble, BP 53, 38041 Grenoble Cedex 09, France*
[2]*Department of Physics and Astronomy, University College London, Gower Street, London WC1E 6BT*

ABSTRACT
Rotational excitation of H_2O, HDO and D_2O by thermal electron impact is studied using the molecular **R**-matrix method. Rate coefficients are obtained up to electron temperatures of 8000 K. De-excitation rates and critical electron densities are also given. It is shown that the dominant transitions are those for which $\Delta J = 0, \pm 1$, as predicted by the dipolar Born approximation. However, a pure Born treatment is found to overestimate the cross-sections close to threshold energies and to neglect important (dipole forbidden) transitions, owing to the importance of short-range and threshold effects. In the context of cometary water, the contribution of electron collisions might explain the need for large H_2O–H_2O collisional excitation rates in population models that neglect electrons.

Key words: molecular data – molecular processes – ISM: molecules.

1 INTRODUCTION

Water vapour has been detected in a great variety of astronomical objects using both spacecraft and Earth-based observations. The *Infrared Space Observatory* (*ISO*), in particular, has revealed the ubiquity of water in the interstellar medium, from star-forming regions (e.g. Wright et al. 2000) to envelopes of evolved stars (e.g. Herpin & Cernicharo 2000). In such environments, water is one of the most abundant molecules, after H_2 and CO, and it plays a critical role in the cooling of the molecular gas. The *Submillimeter Wave Astronomy Satellite* (*SWAS*) was also able to detect water vapour emission from a wide variety of sources using the single 1_{10}–1_{01} rotational transition at 557 GHz (e.g. Melnick et al. 2001). Water can also be detected at radio wavelengths through maser transitions which are commonly associated with star-forming regions (e.g. Furuya et al. 2003) or extragalactic sources (e.g. Hagiwara, Diamond & Miyoshi 2003). In our own Solar system, water has been detected on Venus (Encrenaz et al. 1995), Mars (Gurwell et al. 2000) and the giant planets (Bergin et al. 2000). Water vapour is also the main constituent of cometary comae (e.g. Neufeld et al. 2000) and, finally, 'hot' water has been detected on the Sun, in the umbrae of large sunspots (Polyansky et al. 1997).

Despite a low cosmological abundance of deuterium, D/H $\approx (1.5–3) \times 10^{-5}$ (Pettini & Bowen 2001), several deuterated molecules have been detected in space [for a recent review see e.g. Ceccarelli (2002)]. In particular, the singly deuterated water HDO has been observed in a variety of objects, from Orion IRc2 (Pardo et al. 2001) to Comet Hale–Bopp (Meier et al. 1998). A number of multiply deuterated molecules have also been detected recently (e.g.

Bacmann et al. 2000), but doubly deuterated water D_2O has yet to be discovered.

As the observed intensities of molecular emission depend on a complex competition between radiative and collisional processes, a good knowledge of state-to-state collisional excitation rates is necessary. In the dense interstellar medium, the most important exciting species is H_2. The modelling of many *SWAS* observations was thus based on the use of the collisional rates computed by Phillips, Maluendes & Green (1996) for the rotational excitation of H_2O by H_2 molecules. Dubernet & Grosjean (2002) have recently extended the work of Phillips et al. (1996) to the very low temperatures ($5 < T < 20$ K) found in cold interstellar clouds.

However, in environments where the electron fraction is larger than about 10^{-5}, electron collisions can dominate the molecular excitation because electron-impact collisional rates exceed those for excitation by neutral species by typically 5 orders of magnitude. This point was investigated in some detail by Xie & Mumma (1992) in the context of cometary water. Based on measurements of the electron abundance in Comet Halley and simple estimates of the collisional rates, Xie & Mumma (1992) have shown that standard excitation models significantly underestimate the importance of collisional excitation by electrons. Thus the rotational temperature of H_2O in cometary comae might be controlled by collisions with electrons rather than with neutral molecules. This view was also supported by observations of other species such as methanol, for instance in Comet Lee (Biver et al. 2000).

Electron-impact excitation of the water molecule has been widely studied, both experimentally and theoretically, for many years. The recent theoretical study by Gianturco et al. (1998a) has shown a good agreement with the available experiments in the energy range 2–50 eV. However, to our best knowledge, no accurate calculation has been performed at lower energies, which are necessary to

⋆E-mail: j.tennyson@ucl.ac.uk

compute rates for temperatures lower than about 2000 K. The aim of the present **R**-matrix study is therefore to provide electron-impact rotational (de-)excitation rates for water and water isotopomers over a broad range of temperature and transitions, for astrophysical use. This study will also help in assessing the differences and similarities between the electron-impact rotational excitation rates for neutral molecules and molecular ions, the latter having already been investigated in detail by our group (Rabadán, Sarpal & Tennyson 1998b; Lim, Rabadán & Tennyson 1999; Faure & Tennyson 2001, 2003). In Section 2, **R**-matrix calculations are described and the procedure used to obtain cross-sections is briefly introduced. In Section 3, both cross-sections and rate coefficients are presented and discussed. Conclusions are given in Section 4.

2 CALCULATIONS

2.1 R-matrix calculations

All calculations were performed using the H_2O wavefunctions developed by Gorfinkiel, Morgan & Tennyson (2002) where full details can be found. **R**-matrix calculations were performed at the equilibrium geometry of H_2O, $r_{OH} = 1.81a_0$ and angle between OH bonds $\alpha = 104°5$, using an **R**-matrix sphere of radius $10a_0$. The molecule in this geometry belongs to the C_{2v} point group. A fixed geometry is appropriate, as previous **R**-matrix studies on molecular ions have shown that rotational excitation cross-sections are rather insensitive to vibrational motion effects (Rabadán, Sarpal & Tennyson 1998a). The total wavefunction was based on a close-coupling expansion that included the seven lowest electronic states of water ($2\,^1A_1$, $1\,^3B_1$, $1\,^1B_1$, $1\,^3A_1$, $1\,^3B_2$ and $1\,^1B_2$). The wavefunctions for these states were generated using a CASCI (complete active space configuration interaction) procedure and averaged natural orbitals. This model gives a ground-state energy of -76.0923 au and a dipole moment of 1.864 D, which is close to the experimental value of 1.854 D (Suresh & Naik 2000). The close-coupling expansion was augmented with terms representing correlation and polarization. The continuum functions were represented by Gaussian-type orbitals optimized to represent Bessel functions, with $l \leqslant 4$ (Faure et al. 2002).

In the fixed-geometry approximation, the HDO and D_2O electronic wavefunctions are identical to those of H_2O. The distinction between the water isotopomers therefore arises from the treatment of the rotational motion. In particular, the molecules have different orientations of the principal axes, rotational excitation thresholds and selection rules. These issues are discussed below.

2.2 Rotational cross-sections

The water molecule and its isotopomers are asymmetric top rotors with three different rotational constants. This means that the rotational excitation process involves transitions between $|J_{K_aK_c}\rangle$ states, where J is the principal quantum number, K_a is the projection of J along the A-axis and K_c is its projection along the C-axis. However, it is often more convenient to use the pseudo-quantum number

$$\tau = K_a - K_c, \tag{1}$$

in particular to express the collisional selection rules. In the following, both notations $|J_{K_aK_c}\rangle$ and $|J_\tau\rangle$ will be used.

The rotational excitation cross-sections were calculated following the procedure implemented in the program POLYDCS (Sanna & Gianturco 1998) for the scattering of an electron from a nonlinear molecule in the fixed-nuclei (FN) approximation [the general theory can be found in the review by Gianturco & Jain (1986)]. In this approach, the cross-section is expressed as a partial-wave expansion within the adiabatic nuclei rotation (ANR) method (Lane 1980). For low partial-waves (here $l \leqslant 4$), the cross-section is computed from the FN **T**-matrices obtained via the **R**-matrix calculations. In the case of dipole allowed transitions, the partial-wave expansion does not converge if the FN approximation is applied as it stands, owing to the very long-range nature of the electron–dipole interaction. To circumvent this problem, the standard procedure is to use the dipolar Born approximation to obtain the cross-section for the high partial-waves not included in the FN **T**-matrices (Crawford & Dalgarno 1971). The final cross-section is then calculated as the sum of two contributions and can be regarded as a short-range correction to the Born approximation. For the calculation of Born cross-sections, the required squared dipole transitions moments were computed from the H_2O, HDO and D_2O line intensities tabulated in the Jet Propulsion Laboratory (JPL) catalogue (Pickett et al. 1998). For dipole forbidden transitions, cross-sections are expected to converge rapidly and can be safely evaluated using FN **T**-matrices only. As the current version of POLYDCS is implemented for $J \leqslant 5$, transitions among all levels up to $J = 5$ only were computed (see Section 3.2). Finally, the known unphysical behaviour of the FN cross-sections near rotational thresholds was corrected using a simple kinematic ratio (Chandra & Temkin 1976; Morrison & Sun 1995). The invalidity of the ANR approximation close to excitation thresholds results from the assumption that the electron loses no energy in the inelastic collision. Note that this threshold correction is not implemented in the standard version of the POLYDCS program. Note also that threshold effects can only be included rigorously in a full rotational close-coupling calculation, which is impractical at the collision energies investigated here (see below) because of the excessively large number of open channels that would need to be considered.

3 RESULTS AND DISCUSSION

3.1 Cross-sections

As discussed by Okamoto, Onda & Itikawa (1993), the comparison with experimental differential cross-sections (DCS) is often the only reliable way for testing calculations. Integral cross-sections deduced from experiments are indeed strongly dependent on the extrapolation procedure used to estimate the small-angle scattering which cannot be detected experimentally. As a result, the measured values of the integral cross-sections for water are systematically smaller than theoretical calculations (Okamoto et al. 1993; Gianturco et al. 1998a).

We have therefore computed the elastic (rotationally summed) DCS for electron scattering from H_2O at the electron energy of 6 eV in order to compare our calculations with the recent experimental results of Johnstone & Newell (1991). As shown in Fig. 1, our calculations reproduce the experimental data very well. They are also in very good agreement with the calculations of Gianturco et al. (1998a), in spite of the differences in the short-range treatments. The good agreement between theory and experiment thus suggests that the simple FN approximation, completed with Born calculations for dipolar transitions, is reliable to compute rotational excitation cross-sections.

Inelastic cross-sections were also reported by Gianturco et al. (1998a) in the energy range 2–50 eV. Calculations for dipolar transitions were shown to be in qualitative agreement with the experimental data of Jung et al. (1982). Furthermore, dipolar cross-sections
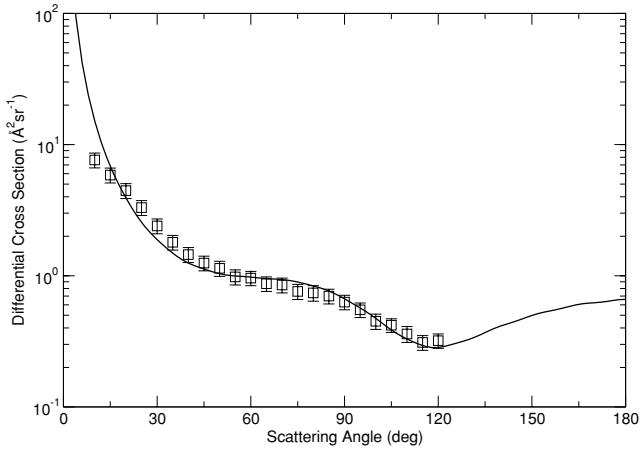
Figure 1. Elastic (rotationally summed) differential cross-section at a collision energy of 6 eV. The squares are experimental points from Johnstone & Newell (1991). The present calculations are given by the solid line.
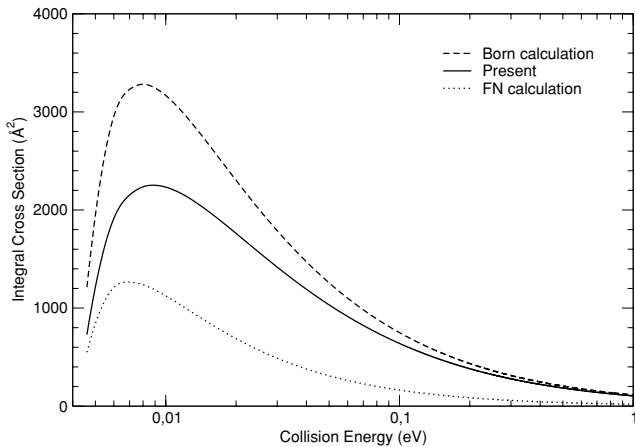

Figure 2. Rotational excitation cross-section for the $0_{00}-1_{11}$ transition in H_2O. Our results are represented by the solid line. The dashed line gives the pure Born caculation. The dotted line gives the FN calculation without the Born completion.

were found to be entirely dominated by high partial-waves, i.e. the short-range correction is negligible. This point was already observed by Jain & Thompson (1983) and was invoked by Xie & Mumma (1992) to justify their use of a pure Born treatment. We did obtain similar results for the same energies. However, as discussed by Clark (1977), the Born approximation is expected to become unreliable close to the threshold energy, i.e. at electron energies lower than about 1 eV, owing to the effects of short-range forces. This is illustrated in Fig. 2, where the Born calculation is shown to overestimate the $0_{00}-1_{11}$ cross-section by about 40 per cent at the peak ($E \approx 0.01\text{eV}$). This point, already observed by Dickinson & Richards (1975) for diatomic polar molecules, clearly shows that short-range and threshold effects are crucial for computing rates at temperatures lower than about 1000 K.

3.2 Rate coefficients

As H_2O has its first electronically excited state, a $^3B_1$, at 7.035 eV, cross-sections were computed in the energy range 0.001–7.0 eV, in order to avoid a high-energy extrapolation procedure. The tran-

sition rates were therefore obtained for temperatures between 100 and 8000 K, assuming a Maxwellian velocity distribution for the electrons. For use in modelling, the temperature dependence of the transition rates, k in $\text{cm}^3 \text{ s}^{-1}$, has been fitted by the analytic form used by Balakrishnan, Forrey & Dalgrano (1999):

$$\log_{10} k(T) = \sum_{n=0}^{N} a_n x^n, \qquad (2)$$

where we have replaced $x = 1/T^{1/3}$ by $x = 1/T^{1/6}$. A fourth-order polynomial ($N = 4$) was found to be sufficient to obtain a reasonable uncertainty over the whole range of temperature $100 \leqslant T \leqslant 8000$ K (see below). It should be noted that the kinematic correction used to force the cross-sections to zero at threshold leads to rate coefficients which do not obey detailed balance at very low temperature. De-excitation rates were therefore computed from the excitation ones using the detailed-balance relation.

The critical electron density, n_{cr}, is defined as the density at which the collisional de-excitation rate is equal to the spontaneous radiative de-excitation rate:

$$n_{\text{cr}}(J_{K_a K_c}, T) = \sum_{J'} \frac{A(J_{K_a K_c} \rightarrow J'_{K'_a K'_c})}{k(J_{K_a K_c} \rightarrow J'_{K'_a K'_c})}. \qquad (3)$$

Note that the usual definition of the critical density refers to a specific transition in a two-level approach. Equation (3) generalizes this concept by considering all relevant transitions involved in the (radiative and collisional) depopulation of a specific rotational level. At densities higher than n_{cr}, electron collisions will maintain rotational levels in Boltzmann equilibrium at the appropriate electron temperature.

3.2.1 H_2O

As the H_2O dipole lies along the axis of intermediate moment of inertia, the selection rules for dipole radiation are (e.g. Gordy & Cook 1984)

$$\Delta J = 0, \pm 1; \quad \Delta K_a = \pm 1, \pm 3, \dots; \quad \Delta K_c = \pm 1, \pm 3, \dots . \quad (4)$$

From equation (4) follows the well-known property that there are two sets of energy levels for H_2O, one with even values of τ (para levels) and one with odd values of τ (ortho levels), between which radiative transitions are highly forbidden. This ortho–para modification results from the quantum statistics of identical particle, here fermions (hydrogen nuclei).

Within the dipolar approximation, Born cross-sections are directly proportional to the squared dipole transition moments (see Section 2.2) and therefore strictly obey the radiative selection rules (4). On the other hand, Jain & Thompson (1983) have discussed electron collisional selection rules for asymmetric top molecules within the FN approximation. They found that transitions are allowed only between symmetric (even τ) states or asymmetric (odd τ) states, which leads to

$$\Delta \tau = 0, \pm 2, \pm 4, \dots . \qquad (5)$$

Thus electron collisions do not interconvert the para- and ortho-forms, as expected.

Rate coefficients for transitions with $\Delta J \leqslant 3$ in para- and ortho-H_2O are presented in Figs 3 and 4, respectively. It can be seen that the largest rates are about $10^{-6} \text{ cm}^3 \text{ s}^{-1}$ and correspond to dipole allowed transitions ($\Delta J = 0, \pm 1$). Transitions with $\Delta J = 2$ are found to be two orders of magnitude smaller and higher transitions lie typically between 10^{-9} and $10^{-11} \text{ cm}^3 \text{ s}^{-1}$. Thus, in contrast to electron-impact rotational excitation of molecular ions for which transitions
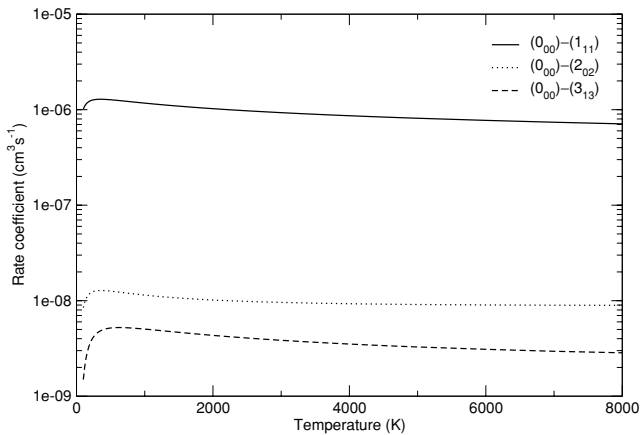
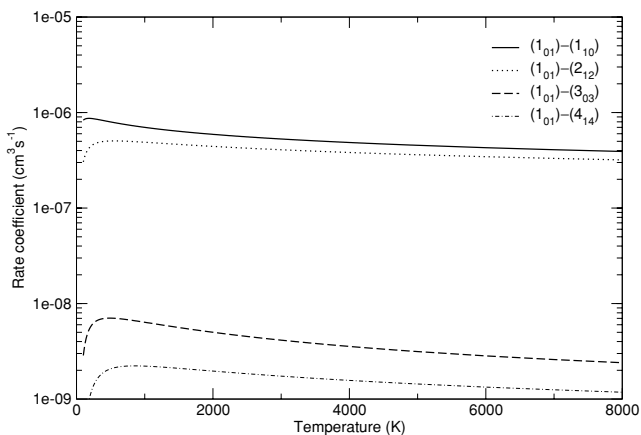**Figure 3.** Rotational excitation rates for para-H_2O.

Figure 4. Rotational excitation rates for ortho-H_2O.

with $\Delta J = 2$ were found in all cases to have rates comparable to (or even larger than) those with $\Delta J = 1$ [see Faure & Tennyson (2003) and references therein], rotational excitation of water is largely dominated by dipolar transitions. In fact, as shown by Faure & Tennyson (2001) in the case of linear molecular ions, the key parameter in the rotational excitation process is the dipole moment value which dictates the magnitude of dipole allowed transitions and, consequently, the relative importance of dipole forbidden transitions. For example, in the case of ozone which has a small dipole moment (0.53 D), Gianturco, Paioletti & Sanna (1998b) found that transitions with $\Delta J = 2$ have cross-sections slightly larger than those with $\Delta J = 1$. This merely reflects the fact that the importance of dipole forbidden transitions is inversely proportional to the dipole moment value of the target (neutral or charged). On the other hand, even in the case of strongly polar molecules, rotational transitions with $\Delta J > 1$ do not have negligible rates. In particular, it is interesting to note that rate coefficients for the rotational excitation of H_2O by neutrals are typically below 10^{-10} cm^3 s^{-1} (Green, Maluendes & McLean 1993; Phillips et al. 1996). This point is further discussed below, in the context of critical densities. Figs 3 and 4 also show that rates peak at relatively high temperatures, between 200 and 1000 K, as a consequence of the large rotational excitation energies of H_2O.

The coefficients of the polynomial fit, equation (2), are given in Tables 1 and 2 for para- and ortho-H_2O, respectively. Rates are

reported for water initially in the lowest five rotational levels, corresponding to $J = 0$, 1 and 2, and for excitation and de-excitation to the lowest eight levels (all those with $J \leqslant 3$). It should be noted that the ratios between specific a_0 coefficients do not necessarily reflect the ratios between the corresponding rates as the relative magnitude of the subsequent polynomial coefficients is crucial. The complete set of fits among all levels up to $J = 5$ is available via the electronic version of this article.[1] Equation (2) was found to reproduce our data within 0.1 per cent for the largest rates and usually within 5 per cent for the smallest rates. We emphasize that these fits are only valid in the temperature range $100 \leqslant T \leqslant 8000$ K.

Critical densities for para- and ortho-H_2O are given in Tables 3 and 4, respectively. These were computed using Einstein A coefficients for spontaneous emission computed from the H_2O line intensities tabulated in the JPL catalogue (Pickett et al. 1998). Note that these A coefficients agree to within 1 per cent with those calculated by Chandra, Varshalovich & Kegel (1984a). Critical electron densities are found to range between 10^3 and 10^6 cm^{-3}, i.e. they are much larger than electron densities in the interstellar medium (typically below 10 cm^{-3}). It is instructive to note that critical H_2 densities, as deduced from the rotational de-excitation rates computed by Phillips et al. (1996) and Dubernet & Grosjean (2002) for the H_2O–H_2 system, range typically between 10^8 and 10^{11} cm^{-3}. This suggests that in any interstellar environments where the electron fraction $n(e)/n(H_2)$ is larger than about 10^{-5}, such as diffuse clouds or photodissociation regions (PDRs), electrons will compete with (or possibly dominate over) neutrals to rotationally excite the water molecules. In this context, it should be noted that H_2O was detected by *ISO* through several rotational lines in the PDR associated with the protoplanetary nebula CRL 618 (Herpin & Cernicharo 2000). Furthermore, in the context of cometary comae where the electron density ranges between 1 and 10^4 cm^{-3} (according to measurements in Comet Halley), current models are based on H_2O–H_2O collisional rates taken to be $\approx 10^{-9}$ cm^3 s^{-1} (e.g. Biver et al. 2000). If poorly known, such a value is likely to be an order of magnitude too large [see e.g. the comparison by Green (1993) between CO–H_2O and CO–He rate coefficients]. Thus critical H_2O densities in comets should be similar to those found for H_2 in the interstellar medium, i.e. around 10^9 cm^{-3}. As $n(e)/n(H_2O)$ is larger than 10^{-3} in cometary comae (Xie & Mumma 1992), the contribution of electron collisions might explain the need for large H_2O–H_2O cross-sections in cometary models that neglect electrons.

3.2.2 D_2O

Like H_2O, D_2O has both ortho- and para- modifications. However, as deuterium nuclei are bosons, the quantum statistics are interchanged with respect to H_2O: para- levels are those with odd values of τ, whereas ortho- levels are those with even τ-values. Radiative and collisional selection rules are, however, unchanged with respect to H_2O since the C_{2v} symmetry is conserved. Moreover, the dipole moment of D_2O is equal to 1.8545 D (Dyke & Muenter 1973), which is very close to the H_2O value (see Section 2.1).

Rate coefficients for transitions with $\Delta J \leqslant 3$ in ortho- and para-D_2O are presented in Figs 5 and 6, respectively. The small differences from H_2O rates (see for comparison Figs 3 and 4) come from the lower rotational excitation energies of D_2O which lead to rates that peak at lower temperatures.

[1] http://www.blackwellpublishing.com/products/journals/suppmat/mnr/mnr7209/mnr7209sm.htm

Table 1. Coefficients a_n ($n = 0$ to 4) of the polynomial fit, equation (2), to the rate coefficients of para-H_2O. The upper level energies, E_{up}, are taken from Pickett et al. (1998). The full version of this table is available at http://www.blackwellpublishing.com/products/journals/suppmat/mnr/mnr7209/mnr7209sm.htm.

Transition	E_{up} (K)	a_0	a_1	a_2	a_3	a_4
(0_{00})–(1_{11})	53.4	−8.020	15.749	−47.137	76.648	−60.191
(0_{00})–(2_{02})	100.9	−5.634	−28.786	116.116	−176.605	76.879
(0_{00})–(2_{11})	137.0	−9.471	−.748	24.714	−39.803	−6.686
(0_{00})–(2_{20})	196.0	−11.259	21.077	−45.756	64.085	−73.978
(0_{00})–(3_{13})	204.7	−9.554	4.930	−4.675	28.113	−72.444
(0_{00})–(3_{22})	296.8	−13.862	29.585	−110.107	234.740	−237.044
(0_{00})–(3_{31})	410.3	−11.805	20.298	−64.372	152.888	−203.031
(1_{11})–(0_{00})	53.4	−8.340	13.414	−33.721	40.549	−19.724
(1_{11})–(2_{02})	100.9	−8.612	15.635	−46.314	74.305	−57.387
(1_{11})–(2_{11})	137.0	−13.543	101.259	−614.594	1440.770	−1174.807
(1_{11})–(2_{20})	196.0	−8.757	20.361	−74.136	143.347	−130.140
(1_{11})–(3_{13})	204.7	−8.487	−2.572	19.436	−12.473	−37.048
(1_{11})–(3_{22})	296.8	−10.539	14.276	−43.962	105.104	−135.032
(1_{11})–(3_{31})	410.3	−13.011	40.432	−139.824	272.664	−264.918
(2_{02})–(0_{00})	100.9	−6.038	−33.192	141.437	−244.736	153.252
(2_{02})–(1_{11})	100.9	−8.696	13.570	−34.435	42.319	−21.511
(2_{02})–(2_{11})	137.0	−8.344	15.050	−43.002	66.415	−49.111
(2_{02})–(2_{20})	196.0	−14.056	50.475	−170.986	288.544	−206.219
(2_{02})–(3_{13})	204.7	−8.600	18.580	−63.602	117.274	−102.297
(2_{02})–(3_{22})	296.8	−12.256	29.234	−79.922	127.233	−117.361
(2_{02})–(3_{31})	410.3	−11.384	26.462	−107.113	238.247	−244.858
(2_{11})–(0_{00})	137.0	−9.767	−6.744	59.160	−132.442	97.108
(2_{11})–(1_{11})	137.0	−13.520	97.607	−593.611	1384.324	−1111.551
(2_{11})–(2_{02})	137.0	−8.238	13.471	−33.930	42.016	−21.774
(2_{11})–(2_{20})	196.0	−8.644	16.050	−49.186	81.660	−65.527
(2_{11})–(3_{13})	204.7	−11.168	22.997	−69.777	118.871	−93.837
(2_{11})–(3_{22})	296.8	−8.960	21.765	−81.238	160.409	−146.991
(2_{11})–(3_{31})	410.3	−13.979	49.629	−175.540	325.826	−279.476
(2_{20})–(0_{00})	196.0	−11.383	12.507	3.507	−68.505	74.686
(2_{20})–(1_{11})	196.0	−8.559	14.114	−38.239	46.761	−21.875
(2_{20})–(2_{02})	196.0	−13.776	46.299	−146.984	223.967	−133.841
(2_{20})–(2_{11})	196.0	−8.469	13.454	−34.265	41.504	−20.506
(2_{20})–(3_{13})	204.7	−9.410	13.017	−31.518	42.144	−25.432
(2_{20})–(3_{22})	296.8	−6.675	−21.201	87.990	−130.157	48.138
(2_{20})–(3_{31})	410.3	−9.041	24.967	−99.051	204.846	−193.371

The coefficients of the polynomial fit, equation (2), are given in Tables 5 and 6 for ortho- and para-D_2O, respectively. Rates are reported for the same transitions as in H_2O and the complete set of fits is also available via the electronic version of this article. As in H_2O, equation (2) was found to reproduce our data within 0.1 per cent for the largest rates and usually within 5 per cent for the smallest rates. Again, we emphasize that these fits are only valid in the temperature range $100 \leqslant T \leqslant 8000$ K.

Critical densities for ortho- and para-D_2O are given in Tables 7 and 8, respectively. These were computed using Einstein A coefficients for spontaneous emission computed from the D_2O line intensities tabulated in the JPL catalogue (Pickett et al. 1998). Critical electron densities for D_2O are found to be one order of magnitude lower than those for H_2O owing mainly to lower Einstein A coefficients but also, at low temperature, to larger rates.

3.2.3 HDO

Besides having moments of inertia intermediate between those of H_2O and D_2O, HDO is of particular importance because its permanent dipole has components along two axes of inertia (Chandra, Kegel & Varshalovich 1984b):

$\mu_a = 0.6567$D (along the A-axis of inertia);

$\mu_b = 1.7318$D (along the B-axis of inertia).

Consequently, in addition to transitions associated with the dipole component parallel to the axis of the intermediate moment of inertia (b-type), as in H_2O and D_2O, there are transitions associated with the dipole component along the axis of the smallest moment of inertia (a-type). These a-type transitions are governed by the selection rules (Gordy & Cook 1984)

$$\Delta J = 0, \pm 1; \quad \Delta K_a = \pm 0, \pm 2, \ldots; \quad \Delta K_c = \pm 1, \pm 3, \ldots, \quad (6)$$

which lead to $\Delta \tau = 1, \pm 3, \ldots$. Since the electronic wavefunction of HDO is identical to those of H_2O and D_2O (in the fixed geometry approximation), a-type transitions are collisionally forbidden in the FN approximation. As a result, a-type cross-sections were evaluated in the Born approximation without short-range correction. Note, however, that short-range and threshold effects are expected to be less important for a-type transitions than for b-type transitions owing to the smaller dipole component (see Dickinson & Richards 1975).

Rate coefficients for transitions with $\Delta J \leqslant 3$ in HDO are presented in Fig. 7. It is observed that rates for the a-type transition 0_{00}–1_{01}

Table 2. Coefficients a_n ($n = 0$ to 4) of the polynomial fit, equation (2), to the rate coefficients of ortho-H_2O. The upper level energies, E_{up}, are taken from Pickett et al. (1998). The full version of this table is available at http://www.blackwellpublishing.com/products/journals/suppmat/mnr/mnr7209/mnr7209sm.htm.

Transition	E_{up} (K)	a_0	a_1	a_2	a_3	a_4
(1_{01})–(1_{10})	61.0	−8.275	15.023	−41.365	61.027	−42.422
(1_{01})–(2_{12})	114.4	−8.443	17.202	−55.589	96.878	−81.189
(1_{01})–(2_{21})	194.1	−12.676	37.113	−114.333	188.989	−152.170
(1_{01})–(3_{03})	196.8	−13.005	38.412	−122.230	207.535	−167.716
(1_{01})–(3_{12})	249.5	−10.282	9.667	−22.319	58.710	−94.323
(1_{01})–(3_{21})	305.3	−5.208	−31.022	98.965	−91.041	−41.194
(1_{01})–(3_{30})	410.6	−12.674	30.750	−109.890	235.491	−252.761
(1_{10})–(1_{01})	61.0	−8.196	13.849	−34.624	42.907	−22.131
(1_{10})–(2_{12})	114.4	−9.465	7.892	−10.545	14.018	−21.601
(1_{10})–(2_{21})	194.1	−8.637	19.823	−71.016	135.514	−122.002
(1_{10})–(3_{03})	196.8	−10.526	9.783	−17.073	33.471	−54.482
(1_{10})–(3_{12})	249.5	−4.125	−39.492	108.481	−78.414	−52.041
(1_{10})–(3_{21})	305.3	−10.270	11.362	−32.407	84.488	−121.253
(1_{10})–(3_{30})	410.6	−12.767	37.835	−128.128	248.959	−245.996
(2_{12})–(1_{01})	114.4	−8.430	13.705	−35.488	42.777	−20.527
(2_{12})–(1_{10})	114.4	−9.529	5.552	2.897	−22.128	18.891
(2_{12})–(2_{21})	194.1	−8.897	16.984	−54.775	95.585	−80.432
(2_{12})–(3_{03})	196.8	−8.635	17.721	−58.025	102.632	−86.288
(2_{12})–(3_{12})	249.5	3.531	−123.453	414.659	−543.401	201.313
(2_{12})–(3_{21})	305.3	−9.253	22.655	−87.951	180.105	−169.763
(2_{12})–(3_{30})	410.6	−14.155	51.131	−184.188	347.406	−301.319
(2_{21})–(1_{01})	194.1	−12.427	30.104	−74.058	80.626	−30.709
(2_{21})–(1_{10})	194.1	−8.467	13.984	−37.459	45.223	−20.795
(2_{21})–(2_{12})	194.1	−8.662	13.492	−34.692	41.504	−19.765
(2_{21})–(3_{03})	196.8	−4.902	−39.717	156.863	−252.388	147.738
(2_{21})–(3_{12})	249.5	−9.168	15.180	−45.233	74.438	−59.634
(2_{21})–(3_{21})	305.3	−12.887	30.826	−86.851	132.476	−101.540
(2_{21})–(3_{30})	410.6	−9.062	25.164	−100.116	207.441	−195.941

Table 3. Critical electron density, n_{cr} in cm^{-3}, as a function of temperature, for rotational levels $J = 1$, 2 and 3 in para-H_2O. Powers of 10 are given in parentheses. The full version of this table is available at http://www.blackwellpublishing.com/products/journals/suppmat/mnr/mnr7209/mnr7209sm.htm.

T (K)	1_{11}	2_{02}	2_{11}	2_{20}	3_{13}	3_{22}	3_{31}
100	3.2(4)	2.2(4)	8.9(3)	4.1(5)	2.6(5)	7.5(5)	4.6(6)
200	3.4(4)	2.3(4)	9.5(3)	4.3(5)	2.7(5)	7.8(5)	4.8(6)
300	3.6(4)	2.4(4)	1.0(4)	4.5(5)	2.9(5)	8.1(5)	5.0(6)
400	3.7(4)	2.6(4)	1.1(4)	4.6(5)	3.0(5)	8.4(5)	5.1(6)
500	3.9(4)	2.7(4)	1.1(4)	4.8(5)	3.1(5)	8.6(5)	5.2(6)
1000	4.4(4)	3.0(4)	1.3(4)	5.3(5)	3.5(5)	9.6(5)	5.8(6)
2000	5.2(4)	3.6(4)	1.5(4)	6.1(5)	4.0(5)	1.1(6)	6.5(6)
3000	5.8(4)	4.0(4)	1.7(4)	6.7(5)	4.4(5)	1.2(6)	7.1(6)
4000	6.3(4)	4.3(4)	1.8(4)	7.2(5)	4.8(5)	1.3(6)	7.6(6)
5000	6.7(4)	4.6(4)	1.9(4)	7.6(5)	5.0(5)	1.4(6)	8.1(6)
6000	7.0(4)	4.8(4)	2.0(4)	8.0(5)	5.3(5)	1.4(6)	8.5(6)
7000	7.4(4)	5.0(4)	2.1(4)	8.4(5)	5.5(5)	1.5(6)	8.8(6)
8000	7.7(4)	5.3(4)	2.2(4)	8.7(5)	5.8(5)	1.5(6)	9.1(6)

Table 4. Critical electron density, n_{cr} in cm^{-3}, as a function of temperature, for rotational levels $J = 1$, 2 and 3 in ortho-H_2O. Powers of 10 are given in parentheses. The full version of this table is available at http://www.blackwellpublishing.com/products/journals/suppmat/mnr/mnr7209/mnr7209sm.htm.

T (K)	1_{10}	2_{12}	2_{21}	3_{03}	3_{12}	3_{21}	3_{30}
100	3.2(3)	1.3(5)	5.0(5)	1.3(5)	2.6(4)	5.1(5)	3.4(6)
200	3.5(3)	1.4(5)	5.2(5)	1.4(5)	2.9(4)	5.4(5)	3.7(6)
300	3.7(3)	1.4(5)	5.4(5)	1.5(5)	3.1(4)	5.6(5)	3.8(6)
400	3.9(3)	1.5(5)	5.5(5)	1.5(5)	3.2(4)	5.7(5)	4.0(6)
500	4.1(3)	1.5(5)	5.7(5)	1.6(5)	3.4(4)	5.9(5)	4.1(6)
1000	4.8(3)	1.7(5)	6.3(5)	1.8(5)	3.9(4)	6.6(5)	4.7(6)
2000	5.7(3)	2.0(5)	7.1(5)	2.1(5)	4.7(4)	7.6(5)	5.4(6)
3000	6.4(3)	2.2(5)	7.8(5)	2.3(5)	5.2(4)	8.4(5)	6.0(6)
4000	7.0(3)	2.3(5)	8.3(5)	2.4(5)	5.7(4)	9.0(5)	6.5(6)
5000	7.5(3)	2.5(5)	8.8(5)	2.6(5)	6.1(4)	9.5(5)	6.9(6)
6000	8.0(3)	2.6(5)	9.3(5)	2.7(5)	6.4(4)	1.0(6)	7.2(6)
7000	8.4(3)	2.7(5)	9.7(5)	2.8(5)	6.7(4)	1.0(6)	7.6(6)
8000	8.7(3)	2.8(5)	1.0(6)	3.0(5)	7.0(4)	1.1(6)	7.9(6)

are lower than those for the *b*-type transition 0_{00}–1_{11}, as expected from the smaller μ_a dipole component. The small differences from H_2O and D_2O rates (see for comparison Figs 3–6) come from the intermediate rotational excitation energies of HDO and the smaller dipole component along the *b*-axis of inertia.

The coefficients of the polynomial fit, equation (2), are given in Tables 9 and 10 for *b*-type and *a*-type transitions, respectively. The complete set of fits is also available via the electronic version of this article. As in H_2O and D_2O, equation (2) was found to reproduce our data within 0.1 per cent for the largest rates and usually within

Table 5. Coefficients a_n ($n = 0$ to 4) of the polynomial fit, equation (2), to the rate coefficients of ortho-D_2O. The upper level energies, E_{up}, are taken from Pickett et al. (1998). The full version of this table is available at http://www.blackwellpublishing.com/products/journals/suppmat/mnr/mnr7209/mnr7209sm.htm.

Transition	E_{up} (K)	a_0	a_1	a_2	a_3	a_4
(0_{00})–(1_{11})	29.2	−7.922	14.675	−40.553	60.641	−43.044
(0_{00})–(2_{02})	51.7	−5.106	−34.706	140.653	−225.482	121.178
(0_{00})–(2_{11})	70.9	−9.286	−3.448	39.563	−77.646	36.629
(0_{00})–(2_{20})	106.6	−11.511	23.486	−50.978	58.224	−45.553
(0_{00})–(3_{13})	107.2	−9.227	.290	20.490	−35.005	−2.977
(0_{00})–(3_{22})	158.3	−13.381	22.668	−72.281	139.338	−133.317
(0_{00})–(3_{31})	225.3	−11.472	14.092	−24.690	41.510	−73.039
(1_{11})–(0_{00})	29.2	−8.313	13.396	−33.209	40.897	−20.931
(1_{11})–(2_{02})	51.7	−8.537	14.502	−39.324	57.573	−39.588
(1_{11})–(2_{11})	70.9	−13.164	97.469	−601.260	1418.918	−1154.578
(1_{11})–(2_{20})	106.6	−8.470	16.822	−53.774	92.894	−77.557
(1_{11})–(3_{13})	107.2	−8.075	−7.925	45.605	−72.825	24.244
(1_{11})–(3_{22})	158.3	−10.153	8.681	−13.271	27.591	−50.236
(1_{11})–(3_{31})	225.3	−12.750	36.028	−110.906	188.124	−161.367
(2_{02})–(0_{00})	51.7	−5.652	−36.972	153.663	−260.453	160.341
(2_{02})–(1_{11})	51.7	−8.693	13.521	−33.684	42.392	−22.567
(2_{02})–(2_{11})	70.9	−8.241	14.200	−37.720	53.873	−35.927
(2_{02})–(2_{20})	106.6	−14.039	49.398	−163.031	265.254	−178.049
(2_{02})–(3_{13})	107.2	−8.397	15.937	−48.297	79.578	−63.012
(2_{02})–(3_{22})	158.3	−12.394	30.406	−80.120	112.371	−82.915
(2_{02})–(3_{31})	225.3	−11.094	19.837	−67.499	136.140	−135.451
(2_{11})–(0_{00})	70.9	−9.776	−6.552	57.404	−125.643	90.421
(2_{11})–(1_{11})	70.9	−13.262	95.627	−590.695	1390.533	−1122.806
(2_{11})–(2_{02})	70.9	−8.184	13.358	−32.877	40.827	−21.286
(2_{11})–(2_{20})	106.6	−8.580	14.966	−42.653	65.837	−48.719
(2_{11})–(3_{13})	107.2	−11.142	22.522	−66.163	107.363	−77.598
(2_{11})–(3_{22})	158.3	−8.665	17.849	−58.764	104.319	−88.238
(2_{11})–(3_{31})	225.3	−13.629	44.307	−145.467	247.523	−192.028
(2_{20})–(0_{00})	106.6	−11.895	18.803	−24.086	−14.079	35.439
(2_{20})–(1_{11})	106.6	−8.463	13.420	−34.231	40.340	−18.680
(2_{20})–(2_{02})	106.6	−13.877	46.981	−149.143	227.902	−136.200
(2_{20})–(2_{11})	106.6	−8.474	13.391	−33.613	41.548	−21.528
(2_{20})–(3_{13})	107.2	−9.327	13.644	−32.405	43.825	−25.346
(2_{20})–(3_{22})	158.3	−6.169	−26.947	112.111	−178.757	92.548
(2_{20})–(3_{31})	225.3	−8.662	19.850	−69.706	130.753	−115.222
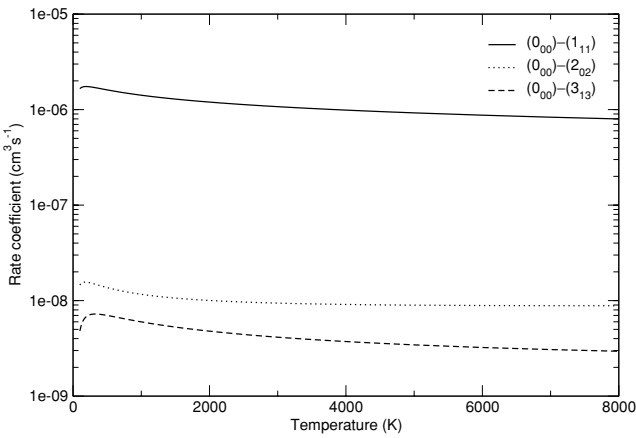
Figure 5. Rotational excitation rates for ortho-D_2O.
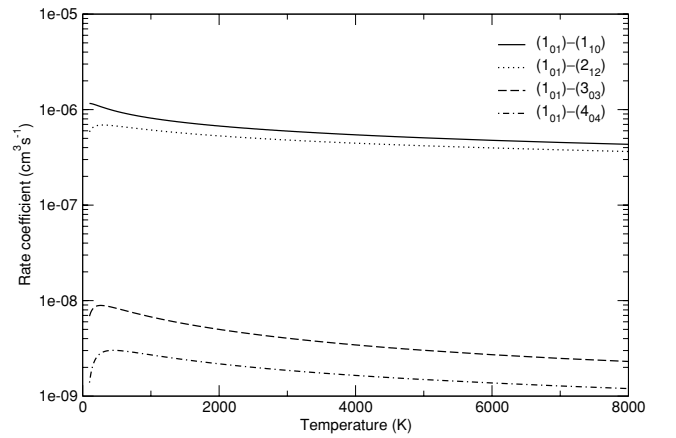
Figure 6. Rotational excitation rates for para-D_2O.

5 per cent for the smallest rates. Again, we emphasize that these fits are only valid in the temperature range $100 \leqslant T \leqslant 8000$ K.

Critical densities for HDO are given in Tables 11 and 12. These were computed using Einstein A coefficients for spontaneous emission computed from the HDO line intensities tabulated in the JPL catalogue (Pickett et al. 1998). Again, note that these A coefficients agree to within 1 per cent with those calculated by Chandra et al. (1984b). Critical electron densities for HDO are found to be

Table 6. Coefficients a_n ($n = 0$ to 4) of the polynomial fit, equation (2), to the rate coefficients of para-D_2O. The upper level energies, E_{up}, are taken from Pickett et al. (1998). The full version of this table is available at http://www.blackwellpublishing.com/products/journals/suppmat/mnr/mnr7209/mnr7209sm.htm.

Transition	E_{up} (K)	a_0	a_1	a_2	a_3	a_4
(1_{01})–(1_{10})	32.7	−8.221	14.589	−38.473	54.265	−34.987
(1_{01})–(2_{12})	60.6	−8.284	15.274	−44.289	69.358	−52.406
(1_{01})–(2_{21})	106.0	−12.526	34.788	−100.427	150.686	−106.139
(1_{01})–(3_{03})	101.3	−12.367	29.737	−79.984	113.772	−80.587
(1_{01})–(3_{12})	128.1	−9.941	4.722	4.723	−9.592	−18.942
(1_{01})–(3_{21})	161.6	−4.851	−37.482	138.806	−194.445	68.154
(1_{01})–(3_{30})	225.5	−12.236	24.025	−70.591	130.830	−134.072
(1_{10})–(1_{01})	32.7	−8.176	13.916	−34.613	43.905	−23.405
(1_{10})–(2_{12})	60.6	−9.400	6.969	−5.532	1.036	−5.876
(1_{10})–(2_{21})	106.0	−8.398	16.707	−53.006	90.887	−75.243
(1_{10})–(3_{03})	101.3	−10.317	6.556	.082	−8.915	−7.641
(1_{10})–(3_{12})	128.1	−3.542	−45.560	132.431	−127.896	.865
(1_{10})–(3_{21})	161.6	−9.907	6.164	−3.394	10.059	−38.443
(1_{10})–(3_{30})	225.5	−12.594	34.417	−103.596	173.188	−149.386
(2_{12})–(1_{01})	60.6	−8.379	13.390	−33.464	40.235	−19.766
(2_{12})–(1_{10})	60.6	−9.539	5.746	1.490	−17.840	15.265
(2_{12})–(2_{21})	106.0	−8.761	15.335	−44.995	71.602	−55.052
(2_{12})–(3_{03})	101.3	−8.485	15.483	−44.941	70.642	−52.903
(2_{12})–(3_{12})	128.1	11.350	−217.574	833.390	−1363.448	804.712
(2_{12})–(3_{21})	161.6	−8.849	17.921	−60.575	110.986	−96.917
(2_{12})–(3_{30})	225.5	−13.737	45.021	−149.753	258.322	−202.924
(2_{21})–(1_{01})	106.0	−12.487	30.909	−78.137	90.719	−38.931
(2_{21})–(1_{10})	106.0	−8.404	13.493	−34.537	41.200	−19.556
(2_{21})–(2_{12})	106.0	−8.627	13.337	−33.514	40.722	−20.454
(2_{21})–(3_{03})	106.0	−4.656	−41.985	163.718	−261.656	152.729
(2_{21})–(3_{12})	128.1	−9.089	13.736	−36.322	52.802	−36.444
(2_{21})–(3_{21})	161.6	−13.331	36.488	−109.326	167.145	−111.437
(2_{21})–(3_{30})	225.5	−8.668	19.866	−69.795	130.971	−115.494

Table 7. Critical electron density, n_{cr} in cm^{-3}, as a function of temperature, for rotational levels $J = 1$, 2 and 3 in ortho-D_2O. Powers of 10 are given in parentheses. The full version of this table is available at http://www.blackwellpublishing.com/products/journals/suppmat/mnr/mnr7209/mnr7209sm.htm.

T (K)	1_{11}	2_{02}	2_{11}	2_{20}	3_{13}	3_{22}	3_{31}
100	4.0(3)	1.7(3)	1.1(3)	5.7(4)	2.8(4)	9.4(4)	6.2(5)
200	4.4(3)	1.9(3)	1.2(3)	6.0(4)	3.1(4)	1.0(5)	6.6(5)
300	4.8(3)	2.0(3)	1.3(3)	6.4(4)	3.3(4)	1.1(5)	6.9(5)
400	5.0(3)	2.2(3)	1.4(3)	6.6(4)	3.5(4)	1.1(5)	7.1(5)
500	5.3(3)	2.3(3)	1.4(3)	6.9(4)	3.7(4)	1.1(5)	7.4(5)
1000	6.2(3)	2.7(3)	1.7(3)	7.9(4)	4.3(4)	1.3(5)	8.3(5)
2000	7.4(3)	3.2(3)	2.0(3)	9.2(4)	5.1(4)	1.5(5)	9.6(5)
3000	8.3(3)	3.6(3)	2.3(3)	1.0(5)	5.7(4)	1.7(5)	1.1(6)
4000	9.0(3)	3.9(3)	2.5(3)	1.1(5)	6.2(4)	1.8(5)	1.1(6)
5000	9.6(3)	4.2(3)	2.7(3)	1.2(5)	6.6(4)	1.9(5)	1.2(6)
6000	1.0(4)	4.5(3)	2.8(3)	1.2(5)	7.0(4)	2.0(5)	1.3(6)
7000	1.1(4)	4.7(3)	3.0(3)	1.3(5)	7.3(4)	2.1(5)	1.3(6)
8000	1.1(4)	4.9(3)	3.1(3)	1.4(5)	7.6(4)	2.2(5)	1.4(6)

Table 8. Critical electron density, n_{cr} in cm^{-3}, as a function of temperature, for rotational levels $J = 1$, 2 and 3 in para-D_2O. Powers of 10 are given in parentheses. The full version of this table is available at http://www.blackwellpublishing.com/products/journals/suppmat/mnr/mnr7209/mnr7209sm.htm.

T (K)	1_{10}	2_{12}	2_{21}	3_{03}	3_{12}	3_{21}	3_{30}
100	4.7(2)	1.5(4)	6.5(4)	1.2(4)	2.5(3)	7.2(4)	2.5(5)
200	5.3(2)	1.7(4)	6.9(4)	1.3(4)	2.8(3)	7.6(4)	2.7(5)
300	5.7(2)	1.8(4)	7.2(4)	1.4(4)	3.0(3)	8.0(4)	2.9(5)
400	6.1(2)	1.8(4)	7.5(4)	1.5(4)	3.2(3)	8.3(4)	3.0(5)
500	6.4(2)	1.9(4)	7.7(4)	1.5(4)	3.4(3)	8.6(4)	3.1(5)
1000	7.7(2)	2.2(4)	8.8(4)	1.8(4)	4.1(3)	9.9(4)	3.6(5)
2000	9.4(2)	2.6(4)	1.0(5)	2.1(4)	4.9(3)	1.2(5)	4.3(5)
3000	1.1(3)	2.9(4)	1.1(5)	2.4(4)	5.6(3)	1.3(5)	4.8(5)
4000	1.2(3)	3.1(4)	1.2(5)	2.6(4)	6.1(3)	1.4(5)	5.2(5)
5000	1.3(3)	3.4(4)	1.3(5)	2.8(4)	6.5(3)	1.5(5)	5.5(5)
6000	1.3(3)	3.5(4)	1.4(5)	2.9(4)	6.9(3)	1.6(5)	5.8(5)
7000	1.4(3)	3.7(4)	1.4(5)	3.1(4)	7.3(3)	1.6(5)	6.1(5)
8000	1.5(3)	3.9(4)	1.5(5)	3.2(4)	7.6(3)	1.7(5)	6.3(5)

intermediate between those for H_2O and D_2O, as expected from the Einstein A coefficients.

4 CONCLUSIONS

We have calculated electron-impact rotational excitation rates for H_2O, HDO and D_2O. These calculations show that such collisions are essentially dominated by dipolar transitions owing to the large dipole moments of water and water isotopomers. However, short-range and threshold effects are important and were included via **R**-matrix results as corrections to the Born approximation. Dipole forbidden transitions thus have appreciable rates which cannot be neglected in any detailed population model of water. In particular, we have shown that rates for electron-impact excitation are crucial

Table 9. Coefficients a_n ($n = 0$ to 4) of the polynomial fit, equation (2), to the rate coefficients of HDO (b-type transitions). The upper level energies, $E_{\rm up}$, are taken from Pickett et al. (1998). The full version of this table is available at http://www.blackwellpublishing.com/products/journals/suppmat/mnr/mnr7209/mnr7209sm.htm.

Transition	$E_{\rm up}$ (K)	a_0	a_1	a_2	a_3	a_4
(0_{00})–(1_{11})	42.9	−8.035	15.268	−44.305	69.412	−52.415
(0_{00})–(2_{02})	66.5	−4.781	−37.448	147.298	−229.519	116.750
(0_{00})–(2_{11})	95.2	−9.352	−2.488	34.299	−64.212	21.040
(0_{00})–(2_{20})	157.3	−12.035	30.329	−83.285	127.604	−107.308
(0_{00})–(3_{13})	144.5	−9.326	1.828	11.949	−13.117	−27.846
(0_{00})–(3_{22})	223.6	−13.612	25.978	−90.309	184.637	−182.569
(0_{00})–(3_{31})	335.2	−11.918	19.884	−55.732	119.577	−157.608
(1_{01})–(1_{10})	46.8	−8.334	15.080	−41.514	60.951	−41.975
(1_{01})–(2_{12})	83.6	−8.423	16.242	−50.028	82.775	−66.303
(1_{01})–(2_{21})	156.7	−12.618	36.219	−109.024	174.492	−135.050
(1_{01})–(3_{03})	131.4	−11.390	17.760	−29.424	22.193	−23.203
(1_{01})–(3_{12})	167.6	−10.037	6.151	−3.342	11.285	−42.722
(1_{01})–(3_{21})	226.0	−5.698	−28.489	103.907	−128.882	12.204
(1_{01})–(3_{30})	335.4	−12.538	28.579	−96.475	198.297	−209.361
(1_{10})–(1_{01})	46.8	−8.263	14.011	−35.371	44.425	−23.450
(1_{10})–(2_{12})	83.6	−9.430	7.396	−7.845	6.954	−12.741
(1_{10})–(2_{21})	156.7	−8.602	18.596	−63.984	117.342	−102.780
(1_{10})–(3_{03})	131.4	−10.315	6.308	.401	−7.182	−12.952
(1_{10})–(3_{12})	167.6	−3.933	−39.128	96.835	−47.978	−65.928
(1_{10})–(3_{21})	226.0	−10.090	8.886	−17.648	44.718	−75.490
(1_{10})–(3_{30})	335.4	−13.051	40.794	−137.214	254.873	−233.408
(1_{11})–(0_{00})	42.9	−8.387	13.401	−33.570	40.504	−19.985
(1_{11})–(2_{02})	66.5	−8.650	14.607	−40.012	58.970	−40.933
(1_{11})–(2_{11})	95.2	−13.266	98.476	−604.736	1424.418	−1159.562
(1_{11})–(2_{20})	157.3	−8.663	18.873	−65.588	121.316	−106.866
(1_{11})–(3_{13})	144.5	−7.990	−8.539	45.876	−67.972	13.757
(1_{11})–(3_{22})	223.6	−10.310	10.951	−25.736	59.222	−85.561
(1_{11})–(3_{31})	335.2	−13.112	41.302	−139.400	259.154	−236.923
(2_{02})–(0_{00})	66.5	−5.285	−40.354	163.995	−274.436	167.086
(2_{02})–(1_{11})	66.5	−8.803	13.581	−34.113	43.087	−23.122
(2_{02})–(2_{11})	95.2	−8.319	14.591	−40.363	59.830	−42.334
(2_{02})–(2_{20})	157.3	−14.176	50.424	−167.514	277.079	−194.764
(2_{02})–(3_{13})	144.5	−8.557	17.103	−55.152	95.922	−79.954
(2_{02})–(3_{22})	223.6	−12.810	36.047	−107.454	172.654	−138.480
(2_{02})–(3_{31})	335.2	−11.690	23.543	−83.805	179.672	−190.301
(2_{11})–(0_{00})	95.2	−9.771	−6.649	58.211	−128.557	93.172
(2_{11})–(1_{11})	95.2	−13.334	96.190	−591.597	1389.052	−1119.910
(2_{11})–(2_{02})	95.2	−8.235	13.331	−33.122	40.348	−20.496
(2_{11})–(2_{20})	157.3	−8.773	16.009	−49.207	81.530	−65.705
(2_{11})–(3_{13})	144.5	−11.237	23.710	−71.345	118.232	−88.120
(2_{11})–(3_{22})	223.6	−8.915	20.377	−73.055	138.813	−123.401
(2_{11})–(3_{31})	335.2	−13.794	46.711	−160.619	291.055	−245.612
(2_{12})–(1_{01})	83.6	−8.465	13.563	−34.634	41.355	−19.871
(2_{12})–(1_{10})	83.6	−9.544	5.789	1.394	−17.918	15.152
(2_{12})–(2_{21})	156.7	−8.923	16.606	−52.647	89.856	−74.341
(2_{12})–(3_{03})	131.4	−8.646	16.059	−48.174	77.920	−59.990
(2_{12})–(3_{12})	167.6	13.375	−240.408	929.513	−1545.037	931.738
(2_{12})–(3_{21})	226.0	−9.015	20.350	−74.416	144.675	−131.498
(2_{12})–(3_{30})	335.4	−13.873	47.283	−164.107	300.199	−255.413
(2_{20})–(0_{00})	157.3	−12.271	23.437	−43.691	21.102	12.039
(2_{20})–(1_{11})	157.3	−8.549	13.876	−36.862	43.989	−20.149
(2_{20})–(2_{02})	157.3	−13.909	46.439	−144.620	215.497	−125.753
(2_{20})–(2_{11})	157.3	−8.590	13.284	−33.553	39.429	−18.530
(2_{20})–(3_{13})	157.3	−9.497	14.139	−35.519	46.793	−26.012
(2_{20})–(3_{22})	223.6	−5.842	−29.884	120.126	−186.151	90.886
(2_{20})–(3_{31})	335.2	−8.968	23.226	−88.793	177.555	−163.622
(2_{21})–(1_{01})	156.7	−12.445	30.335	−75.210	83.506	−33.055
(2_{21})–(1_{10})	156.7	−8.500	13.780	−36.309	42.874	−19.302
(2_{21})–(2_{12})	156.7	−8.708	13.401	−34.226	40.287	−18.773
(2_{21})–(3_{03})	156.7	−4.399	−44.053	168.115	−264.087	150.443
(2_{21})–(3_{12})	167.6	−9.147	13.190	−33.019	45.370	−28.666
(2_{21})–(3_{21})	226.0	−13.674	42.012	−135.927	222.585	−155.800
(2_{21})–(3_{30})	335.4	−8.972	23.250	−88.920	177.860	−163.948

Table 10. Coefficients a_n ($n = 0$ to 4) of the polynomial fit, equation (2), to the rate coefficients of HDO (*a*-type transitions). The upper level energies, E_{up}, are taken from Pickett et al. (1998). The full version of this table is available at http://www.blackwellpublishing.com/products/journals/suppmat/mnr/mnr7209/mnr7209sm.htm.

Transition	E_{up} (K)	a_0	a_1	a_2	a_3	a_4
(0_{00})–(1_{01})	22.3	−8.783	14.405	−38.198	56.488	−39.150
(1_{01})–(0_{00})	22.3	−9.194	13.428	−32.585	41.394	−22.240
(1_{01})–(2_{02})	66.5	−9.033	15.147	−43.119	69.092	−53.424
(1_{01})–(2_{20})	157.3	−11.610	19.207	−67.362	131.445	−121.555
(1_{10})–(1_{11})	46.8	−8.985	13.735	−32.889	42.962	−23.560
(1_{10})–(2_{11})	95.2	−9.182	15.468	−44.970	73.653	−58.095
(1_{11})–(1_{10})	46.8	−8.997	13.911	−33.888	45.629	−26.530
(1_{11})–(2_{12})	83.6	−9.144	15.015	−42.271	66.886	−50.943
(2_{02})–(1_{01})	66.5	−9.127	13.229	−32.084	39.373	−20.081
(2_{02})–(2_{21})	156.7	−11.459	17.190	−55.449	100.672	−87.977
(2_{02})–(3_{03})	131.4	−9.155	16.019	−48.463	82.755	−68.459
(2_{02})–(3_{21})	226.0	−11.436	20.393	−74.280	149.324	−140.935
(2_{11})–(1_{10})	95.2	−9.261	13.350	−32.796	40.897	−21.374
(2_{11})–(2_{12})	95.2	−9.492	13.709	−33.558	44.177	−24.836
(2_{11})–(3_{12})	167.6	−9.236	16.471	−51.083	89.330	−75.353
(2_{11})–(3_{30})	335.4	−12.518	24.262	−96.797	207.880	−204.599
(2_{12})–(1_{11})	83.6	−9.247	13.235	−32.042	39.364	−20.094
(2_{12})–(2_{11})	95.2	−9.527	14.219	−36.487	52.054	−33.660
(2_{12})–(3_{13})	144.5	−9.195	15.959	−48.001	81.439	−66.728
(2_{12})–(3_{31})	335.2	−12.668	24.804	−99.952	216.128	−213.600
(2_{20})–(1_{01})	157.3	−11.435	13.299	−33.413	40.101	−19.166
(2_{20})–(2_{21})	157.3	−8.841	14.232	−34.322	46.708	−26.916
(2_{20})–(3_{03})	157.3	−11.619	13.412	−32.607	41.237	−21.990
(2_{20})–(3_{21})	226.0	−9.428	16.336	−50.270	87.257	−73.069
(2_{21})–(2_{02})	156.7	−11.193	13.226	−32.679	39.424	−19.340
(2_{21})–(2_{20})	157.3	−8.842	14.253	−34.440	47.028	−27.280
(2_{21})–(3_{22})	223.6	−9.412	16.115	−49.038	84.228	−70.057
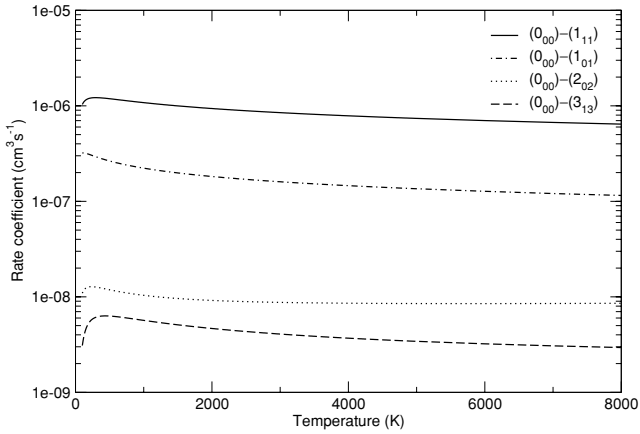
Figure 7. Rotational excitation rates for HDO.

Table 11. Critical electron density, n_{cr} in cm^{-3}, as a function of temperature, for rotational levels $J = 1$ and 2 in HDO. Powers of 10 are given in parentheses.

T (K)	1_{01}	1_{10}	1_{11}	2_{02}	2_{11}	2_{12}	2_{20}	2_{21}
100	1.3(3)	1.8(3)	1.6(4)	5.5(3)	6.8(3)	4.5(4)	8.9(5)	5.3(5)
200	1.5(3)	2.1(3)	1.7(4)	6.1(3)	7.4(3)	4.8(4)	1.0(6)	5.5(5)
300	1.6(3)	2.2(3)	1.8(4)	6.6(3)	7.9(3)	5.1(4)	1.1(6)	5.7(5)
400	1.7(3)	2.4(3)	1.9(4)	6.9(3)	8.3(3)	5.3(4)	1.2(6)	5.8(5)
500	1.8(3)	2.5(3)	1.9(4)	7.3(3)	8.7(3)	5.5(4)	1.2(6)	6.0(5)
1000	2.2(3)	2.9(3)	2.2(4)	8.6(3)	1.0(4)	6.3(4)	1.5(6)	6.6(5)
2000	2.8(3)	3.6(3)	2.6(4)	1.0(4)	1.2(4)	7.3(4)	1.8(6)	7.6(5)
3000	3.1(3)	4.0(3)	2.9(4)	1.2(4)	1.3(4)	8.1(4)	2.0(6)	8.3(5)
4000	3.5(3)	4.4(3)	3.2(4)	1.3(4)	1.5(4)	8.8(4)	2.2(6)	8.8(5)
5000	3.7(3)	4.7(3)	3.4(4)	1.4(4)	1.6(4)	9.4(4)	2.3(6)	9.4(5)
6000	4.0(3)	5.0(3)	3.5(4)	1.4(4)	1.7(4)	9.9(4)	2.4(6)	9.8(5)
7000	4.2(3)	5.3(3)	3.7(4)	1.5(4)	1.7(4)	1.0(5)	2.6(6)	1.0(6)
8000	4.4(3)	5.5(3)	3.9(4)	1.6(4)	1.8(4)	1.1(5)	2.7(6)	1.1(6)

for modelling environments where the electron fraction is larger than about 10^{-5}. In this context, we note the interesting suggestion by Strelnitskij (1984) that electron collisions might contribute to the pumping of H_2O masers which are commonly observed in star-forming regions or active galactic nuclei (AGN). For example, Elitzur & Fuqua (1989) have presented detailed calculations in which the pumping of H_2O masers by collisions with neutrals and electrons can result in arbitrarily high brightness temperatures, provided that the electrons are cooler than the neutrals. As these cal-

culations were based on very simple estimates of the cross-sections for electron collisions, use of the present and higher transition rates should help to assess and clarify the exact role of electrons in cosmic H_2O masers. We are thus at present extending the POLYDCS code of Sanna & Gianturco (1998) to consider rotational levels with $J > 5$, in preparation for the modelling of the important 6_{16}–5_{13} maser transition at 22 GHz.

Table 12. Critical electron density, n_{cr} in cm^{-3}, as a function of temperature, for rotational levels $J = 3$ in HDO. Powers of 10 are given in parentheses. This table is extended to include $J = 4$ and 5 at http://www.blackwellpublishing.com/products/journals/suppmat/mnr/mnr7209/mnr7209sm.htm.

T (K)	3_{03}	3_{12}	3_{13}	3_{21}	3_{22}	3_{30}	3_{31}
100	2.8(4)	3.8(4)	9.6(4)	2.8(6)	1.2(6)	3.2(6)	2.0(7)
200	3.0(4)	4.2(4)	1.0(5)	3.1(6)	1.2(6)	3.8(6)	2.1(7)
300	3.2(4)	4.6(4)	1.1(5)	3.3(6)	1.3(6)	4.2(6)	2.2(7)
400	3.4(4)	4.8(4)	1.1(5)	3.4(6)	1.3(6)	4.6(6)	2.2(7)
500	3.5(4)	5.1(4)	1.2(5)	3.6(6)	1.4(6)	4.8(6)	2.3(7)
1000	4.0(4)	6.0(4)	1.3(5)	4.1(6)	1.5(6)	5.9(6)	2.5(7)
2000	4.8(4)	7.2(4)	1.5(5)	4.9(6)	1.8(6)	7.3(6)	2.8(7)
3000	5.3(4)	8.0(4)	1.7(5)	5.4(6)	1.9(6)	8.3(6)	3.1(7)
4000	5.8(4)	8.8(4)	1.8(5)	5.9(6)	2.1(6)	9.1(6)	3.3(7)
5000	6.2(4)	9.4(4)	2.0(5)	6.3(6)	2.2(6)	9.7(6)	3.5(7)
6000	6.5(4)	9.9(4)	2.1(5)	6.6(6)	2.3(6)	1.0(7)	3.7(7)
7000	6.9(4)	1.0(5)	2.2(5)	6.9(6)	2.4(6)	1.1(7)	3.8(7)
8000	7.1(4)	1.1(5)	2.3(5)	7.2(6)	2.5(6)	1.1(7)	4.0(7)

ACKNOWLEDGMENTS

REFERENCES

Bacmann A., Lefloch B., Ceccarelli C., Steinacker J., Castets A., Loinard L., 2003, ApJ, 585, L55
Balakrishnan N., Forrey R. C., Dalgrano A., 1999, ApJ, 514, 520
Bergin E. A. et al., 2000, ApJ, 539, L147
Biver N. et al., 2000, AJ, 120, 1554
Ceccarelli C., 2002, Planet. Space Sci., 50, 1267
Chandra M., Temkin A., 1976, Phys. Rev. A, 13, 188
Chandra S., Varshalovich D. A., Kegel W. H., 1984a, A&AS, 55, 51
Chandra S., Kegel W. H., Varshalovich D. A., 1984b, A&AS, 58, 687
Clark C. W., 1977, Phys. Rev. A, 16, 1419
Crawford O. H., Dalgarno A., 1971, J. Phys. B: At. Mol. Phys., 4, 494
Dickinson A. S., Richards D., 1975, J. Phys. B: At. Mol. Phys., 17, 2846
Dubernet M. L., Grosjean A., 2002, A&A, 390, 793
Dyke D. R., Muenter J. S., 1973, J. Chem. Phys., 59, 3125
Elitzur M., Fuqua J. B., 1989, ApJ, 347, L35
Encrenaz T., Lellouch E., Cernicharo J., Paubert G., Gulkis S., Spilker T., 1995, Icarus, 117, 164
Faure A., Tennyson J., 2001, MNRAS, 325, 443
Faure A., Tennyson J., 2003, MNRAS, 340, 468
Faure A., Gorfinkiel J. D., Morgan L. A., Tennyson J., 2002, Comput. Phys. Commun., 144, 224
Furuya R. S., Kitamura Y., Wootten A., Claussen M. J., Kawabe R., 2003, ApJS, 144, 71
Gianturco F. A., Jain A., 1986, Phys. Rep., 143, 347
Gianturco F. A., Meloni S., Paioletti P., Lucchese R. R., Sanna N., 1998a, J. Chem. Phys., 108, 4002
Gianturco F. A., Paioletti P., Sanna N., 1998b, Phys. Rev. A, 58, 4484
Gordy W., Cook R. L., 1984, Microwave molecular spectra. John Wiley & Sons, Inc., New York
Gorfinkiel J. D., Morgan L. A., Tennyson J., 2002, J. Phys. B: At. Mol. Opt. Phys., 35, 543
Green S., 1993, ApJ, 412, 436
Green S., Maluendes S., McLean A. D., 1993, ApJS, 85, 181
Gurwell M. A. et al., 2000, ApJ, 539, L143
Hagiwara Y., Diamond P. J., Miyoshi M., 2003, A&A, 400, 457
Herpin F., Cernicharo J., 2000, ApJ, 530, L129
Jain A., Thompson D. G., 1983, J. Phys. B: At. Mol. Phys., 16, 3077
Johnstone W. M., Newell W. R., 1991, J. Phys. B: At. Mol. Opt. Phys., 24, 3633
Jung K., Antoni Th., Muller R., Kochem K.-H., Ehrhardt H., 1982, J. Phys. B: At. Mol. Phys., 15, 3535
Lane N. F., 1980, Rev. Mod. Phys., 52, 29
Lim A., Rabadán I., Tennyson J., 1999, MNRAS, 306, 473
Meier R., Owen T. C., Matthews H. E., Jewitt D. C., Bockelée-Morvan D., Biver N., Crovisier J., Gautier D., 1998, Sci, 279, 842
Melnick G. J., Neufeld D. A., Ford K. E. S., Hollenbach D. J., Ashby M. L. N., 2001, Nat, 412, 160
Morrison M. A., Sun W., 1995, in Huo W. M., Gianturco F. A., eds, Computational Methods for Electron–Molecule Collisions. Plenum Press, New York, p. 131
Neufeld D. A. et al., 2000, ApJ, 539, L151
Okamoto Y., Onda K., Itikawa Y., 1993, J. Phys. B: At. Mol. Opt. Phys., 26, 745
Pardo J. R., Cernicharo J., Herpin F., Kawamura J., Kooi J., Phillips T. G., 2001, ApJ, 562, 799
Pettini M., Bowen D. V., 2001, ApJ, 560, 41
Phillips T. R., Maluendes S., Green S., 1996, ApJS, 107, 467
Pickett H. M., Poynter R. L., Cohen E. A., Delitsky M. L., Pearson J. C., Muller H. S. P., 1998, J. Quant. Spectrosc. Radiat. Transfer, 60, 883
Polyansky O. L., Zobov N. F., Viti S., Tennyson J., Bernath P. F., Wallace L., 1997, Sci, 277, 346
Rabadán I., Sarpal B. K., Tennyson J., 1998a, J. Phys. B: At. Mol. Opt. Phys., 31, 2077
Rabadán I., Sarpal B. K., Tennyson J., 1998b, MNRAS, 299, 171
Sanna N., Gianturco F. A., 1998, Comput. Phys. Commun., 114, 142
Strelnitskij V. S., 1984, MNRAS, 207, 339
Suresh S. J., Naik V. M., 2000, J. Chem. Phys., 113, 9727
Wright C. M., van Dishoeck E. F., Black J. H., Feuchtgruber H., Cernicharo J., González-Alfonso E., de Graauw T., 2000, A&A, 358, 689
Xie X., Mumma M. J., 1992, ApJ, 386, 720

This paper has been typeset from a TEX/LATEX file prepared by the author.